Human Molecular Genetics, 2020, Vol. 29, No. 7 1121–1131

doi: 10.1093/hmg/ddaa018
Advance Access Publication Date: 29 January 2020
General Article

GENERAL ARTICLE

A mouse model for kinesin family member 11 (Kif11)-associated familial exudative vitreoretinopathy

Yanshu Wang[1,2], Philip M. Smallwood[1,2], John Williams[1,2] and Jeremy Nathans[1,2,3,4,*]

[1]Department of Molecular Biology and Genetics, Johns Hopkins University School of Medicine, Baltimore, MD 21205, USA, [2]Howard Hughes Medical Institute, Johns Hopkins University School of Medicine, Baltimore, MD 21205, USA, [3]Department of Neuroscience, Johns Hopkins University School of Medicine, Baltimore, MD 21205, USA and [4]Department of Ophthalmology, Johns Hopkins University School of Medicine, Baltimore, MD 21205, USA

*To whom correspondence should be addressed at: Johns Hopkins University School of Medicine, 805 PCTB, 725 North Wolfe Street, Baltimore, MD 21205, USA. Tel: 410-955-4679; Fax: 410-614-0827; Email: jnathans@jhmi.edu

Abstract

During mitosis, Kif11, a kinesin motor protein, promotes bipolar spindle formation and chromosome movement, and during interphase, Kif11 mediates diverse trafficking processes in the cytoplasm. In humans, inactivating mutations in *KIF11* are associated with (1) retinal hypovascularization with or without microcephaly and (2) multi-organ syndromes characterized by variable combinations of lymphedema, chorioretinal dysplasia, microcephaly and/or mental retardation. To explore the pathogenic basis of *KIF11*-associated retinal vascular disease, we generated a *Kif11* conditional knockout (CKO) mouse and investigated the consequences of early postnatal inactivation of *Kif11* in vascular endothelial cells (ECs). The principal finding is that postnatal EC-specific loss of *Kif11* leads to severely stunted growth of the retinal vasculature, mildly stunted growth of the cerebellar vasculature and little or no effect on the vasculature elsewhere in the central nervous system (CNS). Thus, in mice, Kif11 function in early postnatal CNS ECs is most significant in the two CNS regions—the retina and cerebellum—that exhibit the most rapid rate of postnatal growth, which may sensitize ECs to impaired mitotic spindle function. Several lines of evidence indicate that these phenotypes are not caused by reduced beta-catenin signaling in ECs, despite the close resemblance of the *Kif11* CKO phenotype to that caused by EC-specific reductions in beta-catenin signaling. Based on prior work, defective beta-catenin signaling had been the only known mechanism responsible for monogenic human disorders of retinal hypovascularization. The present study implies that retinal hypovascularization can arise from a second and mechanistically distinct cause.

Introduction

Monogenic disorders in which the retina is insufficiently vascularized are inherited in X-linked, autosomal recessive or autosomal dominant patterns, and they range in severity from subclinical defects in the peripheral retina to congenital blindness secondary to severe retinal gliosis ((1,2); OMIM 13370, 305390, 310600, 605750, 601813 and 613310). Among individuals in which the disease phenotype is confined entirely or predominantly to the retina, 25–30% carry mutations in genes coding for the components of a signaling system in which the Muller glia-derived ligand Norrin binds to receptor Frizzled4 (Fz4), co-receptor Lrp5 and co-activator Tspan12 on the surface of vascular endothelial cells (ECs) to activate beta-catenin signaling ((3–6); beta-catenin signaling is also referred to as canonical Wnt signaling).

Received: July 16, 2019. **Revised:** December 7, 2019. **Accepted:** January 22, 2020

Hemizygous inactivating mutations in the gene coding for Norrin (*NDP*) cause Norrie disease (OMIM 310600), in which severe retinal hypovascularization leads to congenital blindness. Mutations in other beta-catenin pathway genes generally produce a milder degree of hypovascularization, and the resulting phenotypes are referred to as familial exudative vitreoretinopathy (FEVR). In mice, targeted mutations in each of these genes similarly lead to retinal vascularization defects (2,7). In the brain and spinal cord, ligands Wnt7a and Wnt7b, Fz4 and other Frizzled receptors, co-receptors Lrp5 and Lrp6 and co-activators Gpr124 and Reck function analogously to the Norrin/Fz4/Lrp5/Tspan12 system in the retina (8–14). Although the Norrin/Fz4/Lrp5/Tspan12 system is also active in the brain and spinal cord, mutations in genes coding for Norrin signaling components cause relatively mild vascular phenotypes in the brain and spinal cord because of redundancy with Wnt7a/Wnt7b signaling (10,15).

Retinal hypovascularization can also be part of more complex syndromes. For example, Norrie disease is frequently associated with progressive hearing loss and, in a subset of affected individuals, with neuropsychiatric features (16). Whereas heterozygous mutations in *LRP5* cause FEVR (OMIM 601813), homozygous mutations in *LRP5* cause Osteoporosis-Pseudoglioma Syndrome (OMIM 259770), which is characterized by both severe retinal hypovascularization and retarded bone development (17). Recently, heterozygous mutations in the gene coding for beta-catenin (*CTNNB1*) have been identified in individuals with isolated defects in retinal vascularization (FEVR) as well as FEVR accompanied by intellectual disability (18,19). *CTNNB1* mutations have also been found in individuals who exhibit some or all of a distinctive constellation of defects, including intellectual disability, autism spectrum disorder, abnormal craniofacial features, childhood hypotonia, progressive spasticity of the lower limbs and sparse hair ((20–22); OMIM 615075). The diversity of these defects likely reflects the widespread role of beta-catenin signaling in mammalian development and the important role of beta-catenin-cadherin complexes in epithelial integrity (23).

The most recent addition to the set of syndromes that feature retinal hypovascularization is microcephaly, lymphedema and chorioretinal dysplasia (MLCRD) syndrome (OMIM 152950), which is caused by mutations in the gene coding for the kinesin motor protein Kif11 (also known as Kinesin-5, BLM-C or Eg5; (24–31)). As with *CTNNB1* mutations, individuals with *KIF11* mutations can exhibit retinal hypovascularization with or without the other features of MLCRD (4,32–35). During mitosis, Kif11, a plus-end directed motor, interacts with microtubules in the mitotic spindle to promote bipolar spindle formation and separation of duplicated centrosomes (36,37). Kif11 has also been implicated in multiple functions unrelated to the mitotic spindle. Kif11 interacts with ribosomes to enhance translation, possibly by serving as a link to microtubules (38); Kif11 enhances transport of vesicles from the *trans*-Golgi network to the plasma membrane (39); and in postmitotic neurons, Kif11 is involved in cell migration and in axonal and dendritic transport and morphology (40–42). Because of its role in cell division, Kif11 has been intensively studied as a potential target for cancer chemotherapy, and several Kif11 inhibitors are currently in clinical trials (43,44).

The present experiments were undertaken to establish a mouse model of retinal hypovascularization due to *Kif11* deficiency. In previous work, a targeted null allele and a gene trap allele in *Kif11* produced no apparent phenotype when present in the heterozygotes state with a wild-type (WT) allele but caused pre-implantation embryonic lethality in the homozygous state, precluding an analysis of *Kif11* function in vascular development (45,46). To permit cell-type-specific analyses of *Kif11* loss-of-function effects at later ages, we have generated a *Kif11* conditional knockout (CKO) allele. We report here that postnatal EC-specific knockout of *Kif11* leads to a profound hypoplasia of the retinal vasculature and a milder hypoplasia of the cerebellar vasculature. Importantly, EC-specific constitutive activation of beta-catenin signaling—induced by artificially stabilizing beta-catenin—does not rescue the *Kif11* retinal vascular phenotype. These data imply that Kif11 causes retarded retinal vascular development by a mechanism that is independent of the beta-catenin pathway. The *Kif11* conditional allele described here should be useful for genetic dissections of *Kif11* function in the contexts of normal development, for modeling *Kif11* deficiency syndromes and for investigating the effects of Kif11 inhibition in cancer chemotherapy.

Results

Construction and characterization of a *Kif11* CKO mouse line

To construct a $Kif11^{CKO}$ allele, exons 5 and 6 were flanked by *loxP* sites (Fig. 1). Deletion of these two exons leads to a 311 base pair deletion within the *Kif11* coding region, resulting in a frameshift starting at codon 129 of the 1052 codon open reading frame. As a technical point, we note that in the construction of the *Kif11* null allele by Chauvière *et al.* (46), in which exons 2 and 3 were replaced by a *Beta-Geo* reporter/selectable marker, the efficiency of homologous recombination in embryonic stem (ES) cells was ~1/400. As the *Kif11* introns contain multiple regions with dispersed repetitive sequences and some of these sequences are present in the homology arms of the targeting vector designed by Chauvière *et al.* (46), we designed the targeting vector for the $Kif11^{CKO}$ allele to minimize such sequences on the assumption that this would increase the efficiency of correctly targeted events. With the $Kif11^{CKO}$ targeting vector shown in Figure 1, the frequency of correctly targeted events was ~20% as determined by southern blotting of ES cell DNA with flanking probes.

$Kif11^{CKO/CKO}$ mice are healthy and fertile. We used *Sox2-Cre*-mediated germline deletion of *Kif11* exons 5 and 6 to generate a recessive loss-of-function allele ($Kif11^{-}$). We note that this $Kif11^{-}$ allele retains the *Frt-Neo-Frt* (*FNF*) selectable marker 5′ of exon 5 and, therefore, can be distinguished by PCR genotyping from the $Kif11^{-}$ allele generated by Cre-mediated recombination of $Kif11^{CKO}$, which lacks the *FNF* insertion. This distinction was essential for assessing the efficiency of Cre-mediated recombination in $Kif11^{CKO/-}$ retinas, as described below. In a $Kif11^{+/-}$ intercross, no $Kif11^{-/-}$ mice were found among 61 progeny genotyped, consistent with the previously reported embryonic lethality of a conventional *Kif11* null allele. As there is no apparent phenotype associated with a reduction in the number of WT *Kif11* alleles from two to one, we have used both $Kif11^{+/+}$ and $Kif11^{+/-}$ as WT controls in the experiments described below.

Retinal response to ablation of *Kif11* in vascular ECs

To explore the role of *Kif11* in retinal vascular development, which occurs in mice during the first 2 postnatal weeks, we used a single intraperitoneal injection of 4-hydroxytamoxifen (4HT) in $Kif11^{CKO/-}$;*Pdgfb-CreER* mice to initiate Cre-mediated elimination of *Kif11* function in vascular ECs. (*Pdgfb-CreER* is also expressed in some hematopoietic cells; effects of *Kif11* recombination

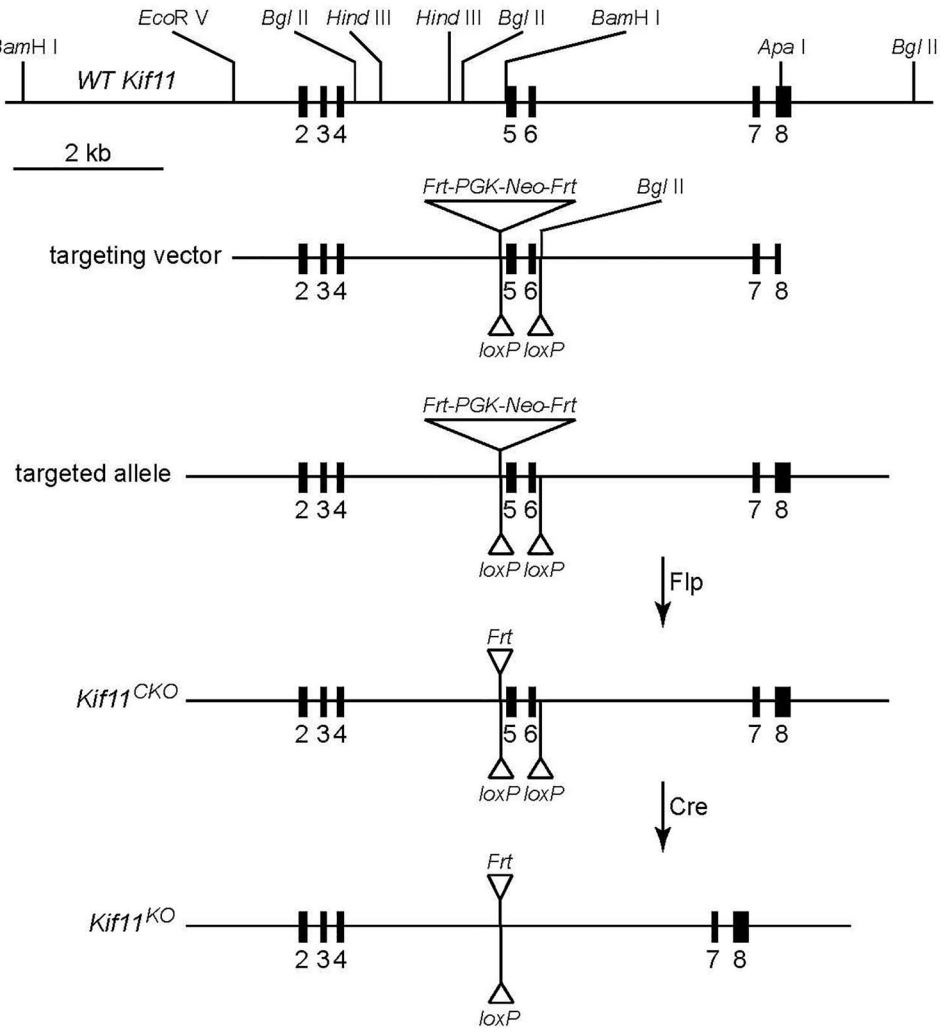

Figure 1. Structure of the *Kif11* CKO allele. Shown from top to bottom are the region of the WT *Kif11* allele encompassing exons 2–8, the ES cell targeting vector, the targeted allele, the CKO allele and the KO allele following the Cre-mediated recombination of the CKO allele.

on hematopoietic cells were not studied.) Retinal flatmounts were prepared from postnatal day (P)8 and P12 *Kif11*$^{CKO/-}$;*Pdgfb-CreER* mice and phenotypically WT littermate controls that had received 100 µg 4HT at P4. This comparison showed that EC-specific loss of *Kif11* produces a severe retardation of retinal vascular development, with reduced radial growth of the vascular front and reduced vascular density within the developing vascular plexus (Fig. 2). This phenotype of retarded angiogenesis is strikingly similar to the retarded angiogenesis produced by the loss of beta-catenin signaling in ECs, as seen in mice lacking *Ndp* or *Fz4* (47–49). Based on analyses of other retinal hypovascularization models (50–52), the retarded vascular development in the *Kif11*$^{CKO/-}$;*Pdgfb-CreER* retina is predicted to cause severe retinal hypoxia.

The severity of the angiogenesis phenotype seen in Figure 2 reflects the efficiency of Cre-mediated recombination. Since *Kif11* is presumed to act cell autonomously, any unrecombined ECs should have continued to proliferate and follow the angiogenic program, as has been observed in mosaic retinas with a mixture of *Frizzled4*$^{+}$ and *Frizzled4* null ECs (48). Our failure to observe mosaic vascular phenotypes in *Kif11*$^{CKO/-}$;*Pdgfb-CreER* retinas implies that, with the 4HT dosage used here, the vast majority of ECs were converted from a *Kif11*$^{CKO/-}$ state to a *Kif11*$^{-/-}$ state.

During the first 2 weeks of postnatal development, the WT murine retinal vasculature develops a blood-retina barrier (BRB), which includes the assembly of tight junctions between ECs and suppression of fenestrae formation and transcytosis (53). These cell biological changes are accompanied by accumulation of the tight junction protein Claudin5 and suppression of Plasmalemma Vesicle-Associated Protein (PLVAP), a structural component of EC fenestrations and caveolae (49,54). In *Kif11*$^{CKO/-}$;*Pdgfb-CreER* retinal ECs at P8, there is an accumulation of PLVAP, especially near the vascular front, which correlates with leakage of the intravascular amine-reactive low molecular weight tracer Sulfo-N-hydroxysuccinimide (NHS)-biotin (Fig. 2A and B). At P12, PLVAP accumulation and Sulfo-NHS-biotin leakage are even more prominent (Fig. 2C and D). Accumulation of PLVAP and increased vascular permeability can occur as a direct effect of reduced beta-catenin signaling, but they can also occur in response to elevated levels of retina-derived vascular endothelial growth factor (VEGF; also known as vascular permeability factor), which is produced at a high level by the hypoxic retina (50,51,55).

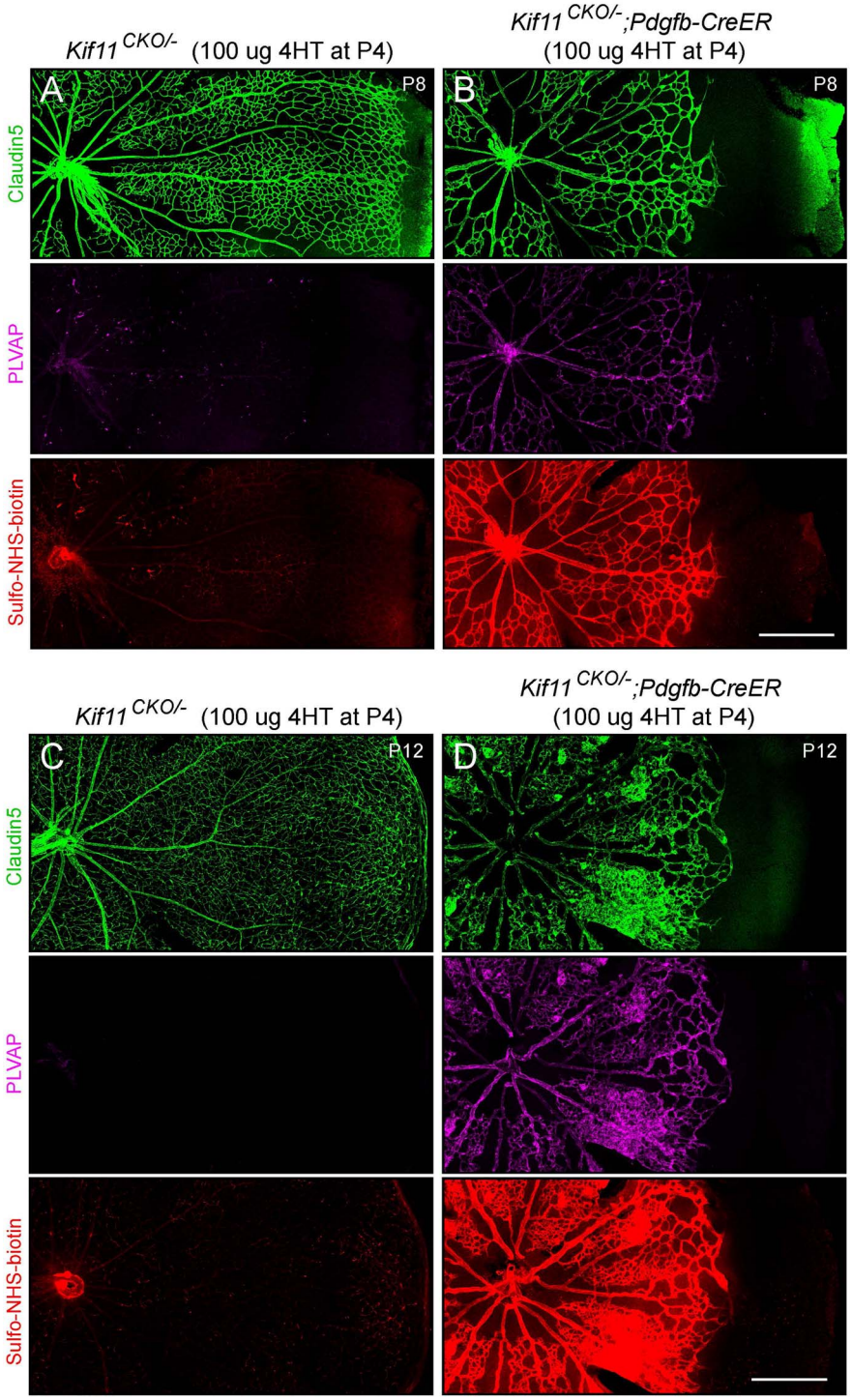

Figure 2. Severely retarded retinal vascular growth following the early postnatal EC-specific knockout of *Kif11*. Retinal flatmounts were prepared at P8 or P12 from littermate control *Kif11*$^{CKO/-}$ mice (**A**,**C**) and *Kif11*$^{CKO/-}$;*Pdgfb-CreER* mice (**B**,**D**) following the treatment with 100 µg 4HT at P4. Each image shows one retinal quadrant, with the optic disc at the left and the retinal periphery at the right. Loss of *Kif11* leads to retarded vascular development and reduced vascular coverage of the retinal surface. At both ages, *Kif11*$^{CKO/-}$;*Pdgfb-CreER* retinas show increased expression of PLVAP and increased Sulfo-NHS-biotin leakage. Scale bars, 500 µm.

Kif11 promotes cell proliferation but not beta-catenin signaling

The retarded angiogenesis phenotype produced by EC-specific loss of Kif11, as described above, could be consistent with either of two models: (1) loss of Kif11 impairs beta-catenin signaling in ECs or (2) loss of Kif11 impairs EC proliferation independent of beta-catenin signaling. As described in the following paragraphs, we have conducted three experimental tests to distinguish these two models.

In the first test, we analyzed the accumulation of LEF1, a transcription factor and beta-catenin partner, in retinal ECs. In addition to functioning as a mediator of beta-catenin signaling,

LEF1 is also a target of beta-catenin regulation, and during retinal and brain vascular development in WT mice, beta-catenin signaling leads to the nuclear accumulation of LEF1 in vein and capillary ECs (Fig. 3A). Under conditions of reduced beta-catenin signaling—as seen in *Ndp* or *Fz4* mutant mice—there is a corresponding reduction in nuclear LEF1 (56,57). In contrast, in *Kif11*$^{CKO/-}$;*Pdgfb-CreER* retinal ECs at P8, LEF1 accumulates in all or nearly all EC nuclei and at levels that are higher than in WT ECs (Fig. 3B), perhaps reflecting feedback regulation produced by retinal hypoxia. These data imply that the beta-catenin pathway is active (and potentially elevated) in ECs in *Kif11*$^{CKO/-}$;*Pdgfb-CreER* retinas. This conclusion is also consistent with the absence of Claudin5 suppression and the relatively modest PLVAP accumulation in *Kif11*$^{CKO/-}$;*Pdgfb-CreER* retinas at P8. In contrast, loss of *Ndp* or *Fz4* (i.e. loss of EC beta-catenin signaling) leads to Claudin5 suppression and high-level accumulation of PLVAP at all postnatal ages (49).

In the second test, we asked whether initiating EC-specific loss of Kif11 in the mature retinal vasculature converts ECs from a Claudin5+/PLVAP− state to a Claudin5−/PLVAP+ state and compromises the BRB, as is observed with acute loss of beta-catenin signaling in mature ECs (49,58). For this test, *Kif11*$^{CKO/-}$;*Pdgfb-CreER* mice were treated with 4HT at P21, when the retinal vasculature was fully developed. When these retinas were examined 10 days later (at P31), the retinal vasculature was still Claudin5+/PLVAP−, and it showed no detectable leakage of intravascular Sulfo-NHS-biotin (Fig. 3C and D). Importantly, the retina flatmount analysis in Figure 3C and D is sufficiently sensitive to detected BBB loss at single-cell resolution because (1) expression of PLVAP in single ECs can be readily observed and (2) loss of barrier integrity by single ECs gives rise to a detectable accumulation of sulfo-NHS-biotin leakage around the affected cells, as demonstrated in Figure 6D of Zhou *et al*. (58).

Since the results described in the preceding paragraph are consistent with either (1) no effect of *Kif11* loss in the mature retinal vasculature or (2) a failure of Cre-mediated recombination in the mature retinal vasculature, it was important to independently assess the presence of Cre-mediated recombination. Therefore, we PCR amplified total retina genomic DNA with primers that distinguish the relevant genotypes to assess Cre-mediated recombination (Supplementary Material, Fig. S1A). Specifically, we used primers that flank the two *Kif11*^{CKO} *loxP* sites and amplified DNA from P31 *Kif11*$^{CKO/-}$;*Pdgfb-CreER* retinas obtained from mice that were injected with 300 μg 4HT at P21, as shown in Figure 3C and D. This reaction generated readily detectable amounts of the ∼550 bp PCR product derived from Cre-mediated recombination of the *Kif11*^{CKO} allele in ECs (Supplementary Material, Fig. S1B, right three lanes), despite the relatively low abundance of EC DNA in the retinal DNA sample (ECs comprise < 5% of retinal cells). In contrast, PCR amplification of DNA from littermate *Kif11*$^{CKO/+}$;*Pdgfb-CreER* or *Kif11*$^{CKO/-}$ retinas that were not exposed to 4HT did not show this product (Supplementary Material, Fig. S1B, left three lanes). Similar results were obtained with seven additional experimental mice and six additional control mice that were injected with 4HT at P4 or P5. We note that under the PCR amplification conditions used here, longer PCR products (e.g. ∼1.2 kb from the unrecombined *Kif11*^{CKO} allele and ∼2.5 kb from the constitutive *Kif11*$^{-}$ allele) do not accumulate to detectable levels. These results imply that a substantial number of *Kif11*$^{CKO/-}$;*Pdgfb-CreER* ECs were converted by Cre-mediated recombination to a *Kif11*$^{-/-}$ genotype at P21. Thus, our failure to observe the conversion of any retinal ECs from PLVAP− to PLVAP+ or any localized sulfo-NHS-biotin leakage implies that loss of *Kif11* in the mature retina has little or no effect on BBB properties.

In the third test, we asked whether constitutive activation of beta-catenin signaling in ECs can rescue the retinal vascular phenotype caused by loss of *Kif11*. In this experiment, 4HT treatment induces Cre-mediated recombination of a *Ctnnb1* allele to generate a deletion derivative that codes for a stabilized version of beta-catenin. More specifically, Cre-mediated deletion of *Ctnnb1* exon 3 leads to a small in-frame deletion that encompasses the phosphorylation site that controls beta-catenin ubiquitination and its subsequent degradation by the proteasome. The *Ctnnb1* allele that has *loxP* sites flanking exon 3 is referred to as *Ctnnb1*^{flex3}. In earlier work that used the same timing and dose of 4HT, *Pdgfb-CreER*-mediated recombination of the *Ctnnb1*^{flex3} allele was observed to fully rescue the retinal vascular defects caused by loss of Norrin (58), which, as described above, closely resembles the defects exhibited by *Kif11*$^{CKO/-}$;*Pdgfb-CreER* retinas. In a WT background, *Pdgfb-CreER*-mediated recombination of the *Ctnnb1*^{flex3} allele has little effect, leading only to a small increase in vascular density (58). For the present experiment, both *Kif11* loss and beta-catenin stabilization were initiated by 4HT treatment at P3. In contrast to the rescue of *Ndp*^{KO} retinas, EC-specific stabilization of beta-catenin had no effect on the *Kif11* loss-of-function phenotype (Fig. 4A–D). At P10, retinas with or without stabilized beta-catenin exhibited indistinguishable patterns of vascular growth retardation (as quantified in Fig. 4E), disorganized capillary structure, and induction of PLVAP. Thus, artificially activating beta-catenin signaling fails to rescue the *Kif11* loss-of-function phenotype.

In sum, these three tests imply that the *Kif11* retinal vascular phenotype is not caused by reduced beta-catenin signaling. The most parsimonious explanation for the *Kif11* phenotype is that it reflects Kif11's role in cell proliferation and, more specifically, in mitotic spindle dynamics during mitosis. In the context of this model, we can explain PLVAP accumulation in ECs and Sulfo-NHS-biotin leakage in *Kif11*$^{CKO/-}$;*Pdgfb-CreER* retinas as secondary consequences of retinal hypoxia rather than as a direct effect of decreased beta-catenin signaling. As noted above, in multiple models of retinal vascular insufficiency, retinal hypoxia results in increased expression of VEGF, which increases PLVAP expression and vascular permeability (50,51,55).

Effect of *Kif11* loss on cerebellar vascular development

We next asked whether EC-specific loss of Kif11 has effects on vascular development beyond the retina. The ∼100% survival of *Kif11*$^{CKO/-}$;*Pdgfb-CreER* mice treated with 4HT at P3–P4 and followed for > 1 week implies that during this period of rapid postnatal growth the vascular supply to most tissues accommodates the increase in demand. As earlier studies had shown highly efficient recombination by *Pdgfb-CreER* throughout the early postnatal brain vasculature (10,15), we focused our comparative analysis on the *Kif11*$^{CKO/-}$;*Pdgfb-CreER* phenotype in the brain. Specifically, we compared sagittal sections of brain from eight *Kif11*$^{CKO/-}$;*Pdgfb-CreER* mice and nine control *Kif11*$^{CKO/-}$ and *Kif11*$^{CKO/+}$ littermates that were treated with 4HT at P3 or P4 and sacrificed between P8 and P12. This analysis showed that the brain sizes between the two cohorts were closely matched, and the vascular densities in the cortex, thalamus, and brain stem were indistinguishable by visual inspection (Fig. 5A and B). However, the cerebella of *Kif11*$^{CKO/-}$;*Pdgfb-CreER* mice showed a modestly reduced vascular density (Fig. 5A–C), an effect that was statistically significant (Fig. 5D). (The *P*-value of 3.9×10^{-4}

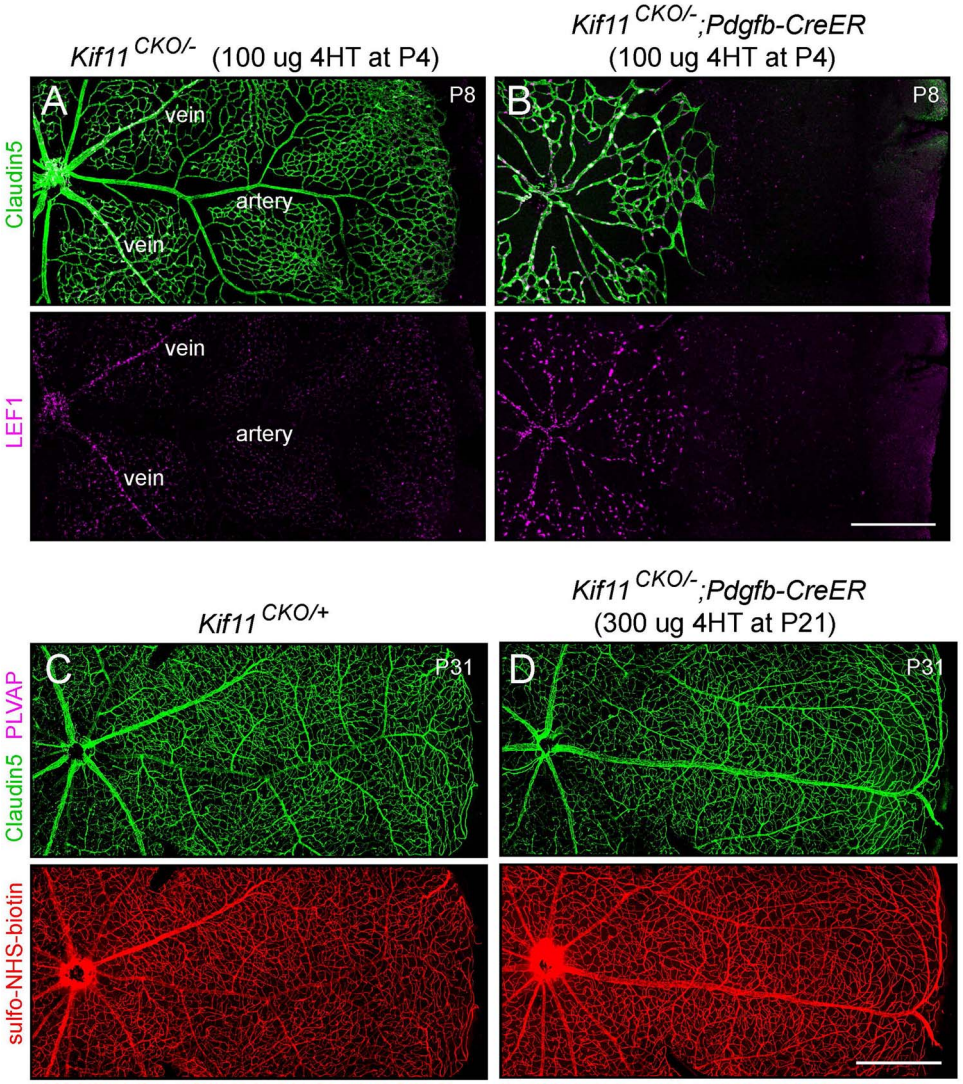

Figure 3. EC-specific knockout of *Kif11* leads to continued EC accumulation of LEF1 during development and no effect of post-mitotic knockout on vascular permeability. (**A**,**B**) Retinal flatmounts were prepared at P8 from littermate control *Kif11*$^{CKO/-}$ mice (A) and *Kif11*$^{CKO/-}$;*Pdgfb-CreER* mice (B) following the treatment with 100 µg 4HT at P4. Each image shows one retinal quadrant, with the optic disc at the left and the retinal periphery at the right. LEF1, a marker of beta-catenin signaling, accumulates in the nuclei of vein and capillary ECs but not in arterial ECs in control retinas and in all ECs in mutant retinas. (**C**,**D**) Retinal flatmounts were prepared at P31 from littermate control *Kif11*$^{CKO/+}$ mice (C) and *Kif11*$^{CKO/-}$;*Pdgfb-CreER* mice (D) following the treatment with 300 µg 4HT at P21. Each image shows one retinal quadrant as in (A) and (B). Loss of *Kif11* has no effect on vascular architecture, expression of Claudin5, suppression of PLVAP or BRB integrity, as seen by the absence of Sulfo-NHS-biotin leakage from the intravascular space into the retinal parenchyma. See Supplementary Material Figure S1 for an analysis of Cre-mediated recombination at P21. Scale bars, 500 µm.

for the experimental versus control comparison in Figure 5D was determined by a conservative calculation in which the comparison was between the mean values of vascular density for individual mice, determined by averaging the fraction of the length of the granule cell layer/molecular layer boundary that was vascularized in seven cerebellar folia per mouse.)

Although the entire brain is growing during early postnatal life in mice, the cerebellum is distinctive in exhibiting extremely rapid growth during this period, with most granule cell divisions and much of the Purkinje cell and granule cell arbor growth occurring postnatally (59). Thus, the early postnatal requirement for Kif11 function in central nervous system (CNS) vascular cells is most significant in two CNS regions—the retina and the cerebellum—that exhibit rapid rates of postnatal growth.

Discussion

The experiments reported here establish a model for *KIF11*-based retinal vascular disease using EC-specific elimination of *Kif11* in mice. The principal finding is that postnatal EC-specific loss of *Kif11* leads to severely stunted growth of the retinal vasculature that is not caused by reduced EC beta-catenin signaling despite its close resemblance to the phenotype caused by mutations in beta-catenin signaling components. Interestingly, one other region of the CNS in which early postnatal EC-specific loss of *Kif11* produces a prominent hypovascularization phenotype is the cerebellum, suggesting that the most significant requirements for Kif11 function occur in rapidly developing CNS regions that require correspondingly rapid vascular growth.

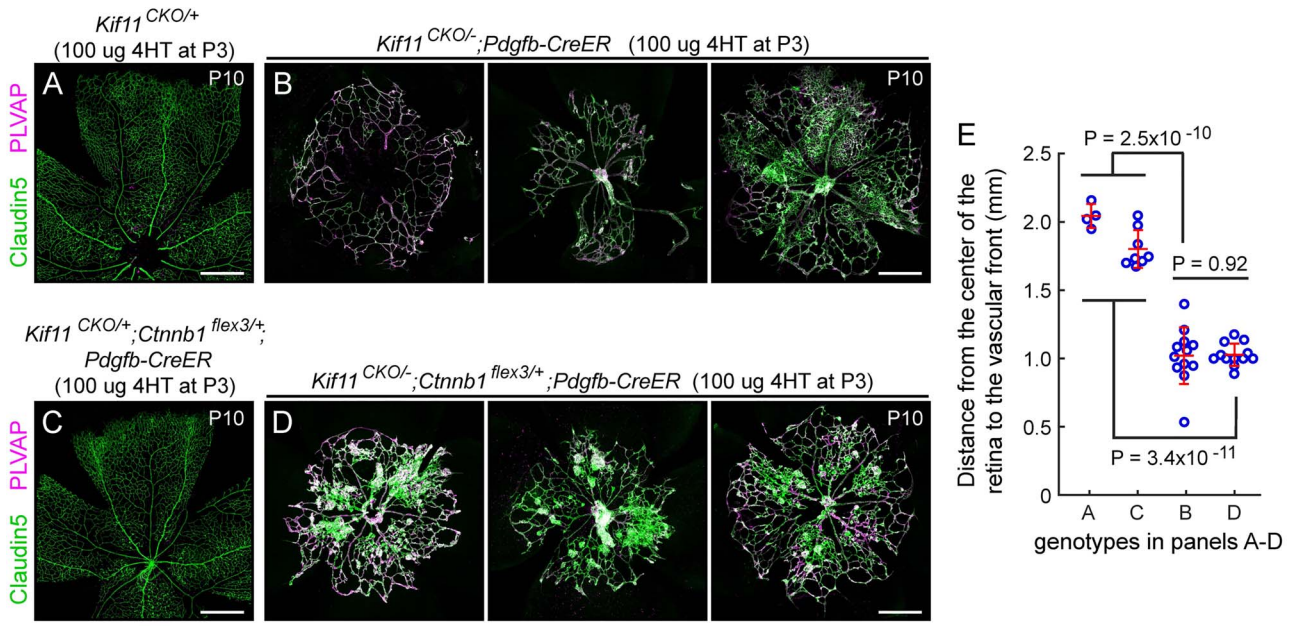

Figure 4. Postnatal EC-specific stabilization of beta-catenin does not rescue the *Kif11* retinal vascular phenotype. (**A**,**B**) Retinal flatmounts were prepared at P10 from control *Kif11*$^{CKO/+}$ mice (A) and *Kif11*$^{CKO/-}$;*Pdgfb-CreER* mice (B; three examples shown) following the treatment with 100 µg 4HT at P3 to assess the *Kif11* retinal vascular phenotype. (**C**,**D**) From the same set of crosses, retinal flatmounts were prepared at P10 from control *Kif11*$^{CKO/+}$;*Ctnnb1*$^{flex3/+}$;*Pdgfb-CreER* mice (C) and *Kif11*$^{CKO/-}$;*Ctnnb1*$^{flex3/+}$;*Pdgfb-CreER* mice (D; three examples shown) following the treatment with 100 µg 4HT at P3. Retinal vascular development in both sets of control mice is indistinguishable from WT. Beta-catenin stabilization following the Cre-mediated recombination of *Ctnnb1*$^{flex3/+}$ fails to rescue the *Kif11* retinal vascular phenotype. In (A) and (C), each image shows one retinal quadrant, with the optic disc at the bottom and the retinal periphery at the top; in (B) and (D), each image is centered on the optic disc. All images in (A–D) are at the same magnification. Scale bars, 500 µm. (**E**) Quantification of the radial distance from the optic disc to the vascular front at P10 for individual retinal quadrants for the genotypes shown in panels A–D. Plots show mean ± standard deviation.

The phenotypic spectrum of *KIF11* disorders

The present work complements a growing literature on the phenotypic consequences of *KIF11* mutations in humans. One set of reports defined a syndrome in which autosomal dominant MLCRD is associated with *KIF11* mutations (25,27). Other studies have noted the extensive overlap with a closely related syndrome characterized by chorioretinal dysplasia, microcephaly and mental retardation, with or without lymphedema that is also associated with *KIF11* mutations (28,30). Finally, analyses that focused on large cohorts of patients with ocular disease have found *KIF11* mutations to be associated with FEVR with or without microcephaly (4,32–35). Taken together, these studies imply a substantial degree of phenotypic variability, potentially related to the diverse functions of Kif11 in mitosis and in intracellular trafficking in non-dividing cells. The present work suggests that reduced Kif11 function in retinal and brain ECs may explain part of the pathophysiology of these human disorders.

The role of *Kif11* in rapidly dividing cells: implications for retinal vascular disease

Kif11, Kif15 (also called Hklp2 or Kinesin-12) and dynein are essential force-generating proteins involved in forming the bipolar spindle during mitosis and directing its movement before and during anaphase (60). Interestingly, Kif15 exhibits partial redundancy with Kif11 in a manner that varies among cell lines (61) and that can account for partial escape from pharmacologic inhibition of Kif11 (62,63). These observations suggest that the rank order of sensitivity of ECs in the early postnatal CNS to loss of Kif11—retina > cerebellum > the rest of the brain—may reflect different degrees of dependence on Kif11 versus Kif15, either as intrinsic differences between the vasculatures in different CNS regions or as functional differences that reflect the rapidity of EC proliferation. In this regard, it is interesting that in experiments aimed at slowing tumor growth with a Kif11 inhibitor, Exertier *et al* (64) observed that Kif11 expression in ECs was increased by VEGF, and that pharmacologic inhibition of Kif11 had potent anti-angiogenic effects in cell culture, in chick and zebrafish embryos, and in a tumor model in mice. Thus, in each of the paradigms in which Kif11 loss or blockade has a large effect, the unifying feature may be the extreme rapidity of EC proliferation.

In sum, the present experiments implicate Kif11's function in mitotic spindle assembly as the likely link to its role in diseases of retinal vascular development, and they suggest that genes coding for other components or regulators of the mitotic spindle could be plausible candidates for diseases or syndromes with the same or overlapping features. Importantly, these data imply that retinal hypovascularization disorders can arise from two mechanistically distinct causes: defects in beta-catenin signaling and defects in the mitotic machinery.

Materials and Methods

Mice

The following mouse alleles were used: *Pdgfb-CreER* (65), *Sox2-Cre* ((66); JAX 008454), *R26-Flp* ((67); JAX 009086), *Ctnnb1*^{flex3} (68), *Kif11*^{CKO} and *Kif11*$^{-}$ (see below). Experiments were conducted, and mice were housed and handled according to the approved Institutional Animal Care and Use Committee protocol MO16M369 of the Johns Hopkins Medical Institutions.

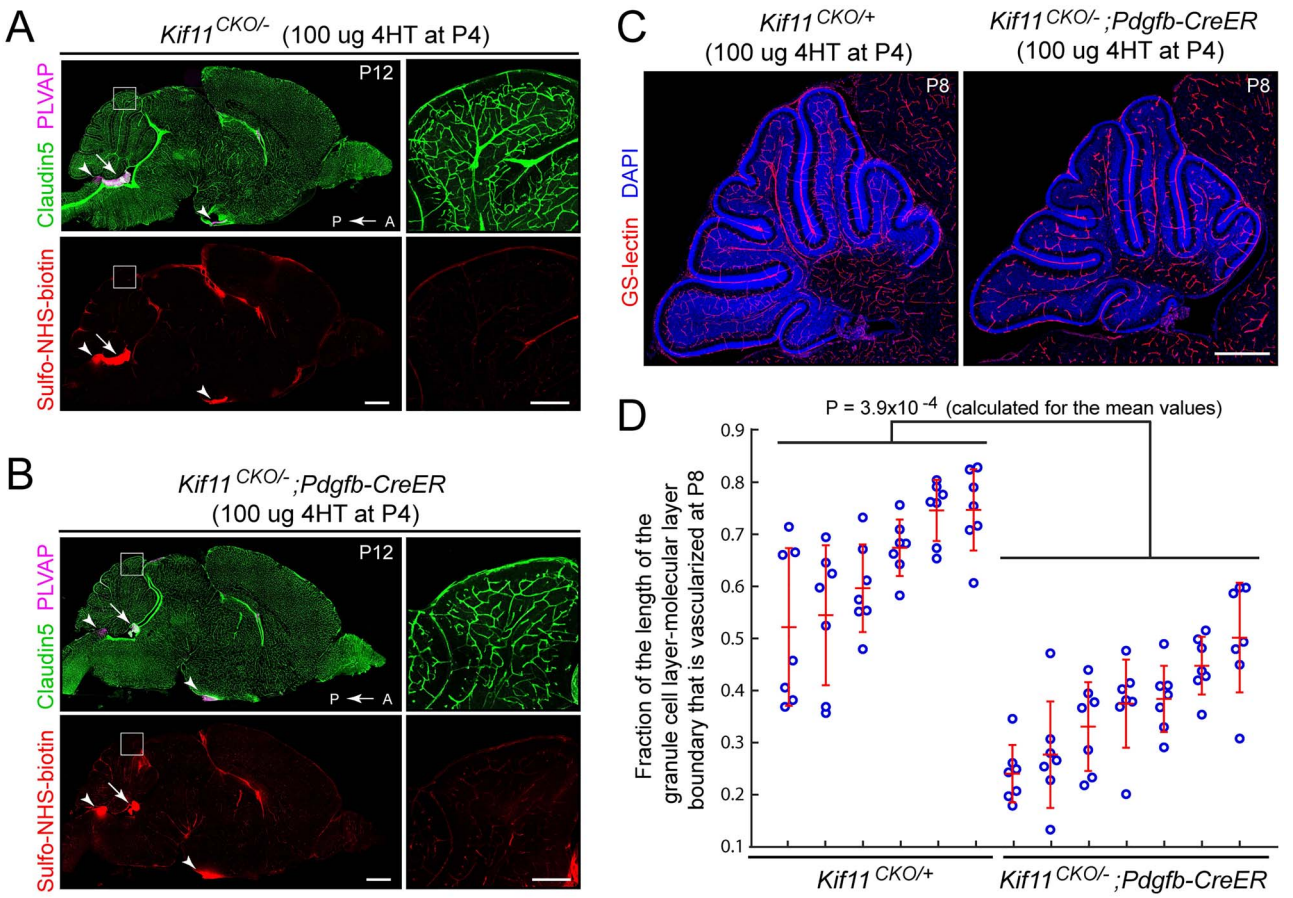

Figure 5. Retarded density of cerebellar vasculature following the early postnatal EC-specific knockout of *Kif11*. (**A**,**B**) Sagittal brain sections were prepared at P12 from control *Kif11*$^{CKO/-}$ mice (A) and *Kif11*$^{CKO/-}$;*Pdgfb-CreER* mice (B) following the treatment with 100 µg 4HT at P4. The region of the dorsal cerebellum enclosed by the white square is enlarged at right. Scale bars, 1 mm (left images) and 200 µm (right images). Except for modestly reduced vascular density in the cerebellum (inset at right), brain size and vascular density are unaffected by EC-specific loss of *Kif11*. Sulfo-NHS-biotin leakage is seen in the choroid plexus (arrow) and in the circumventricular organs (area postrema and median eminence; arrowheads) as expected but is not observed elsewhere in the brain. (**C**) Sagittal brain sections were prepared at P8 from control *Kif11*$^{CKO/+}$ mice and *Kif11*$^{CKO/-}$;*Pdgfb-CreER* mice, following the treatment with 100 µg 4HT at P4. Scale bar, 500 µm. (**D**) With early postnatal loss of *Kif11*, vascular density in the P8 cerebellum is reduced, as determined by quantifying the fraction of the molecular layer/granule cell layer border that is occupied by blood vessels in six control *Kif11*$^{CKO/+}$ and seven *Kif11*$^{CKO/-}$;*Pdgfb-CreER* P8 mice. For each mouse, seven folia were quantified from a single confocal stack of the cerebellum [examples in (C)]. The plot in (D) shows mean ± standard deviation for each mouse.

Construction of the *Kif11* CKO line

A BAC clone with one endpoint 3.5 kb 5′ of exon 2 and extending through the 3′ end of the Kif11 gene was used to construct the targeting vector, which consisted of (1) a ~3.5 kb 5′ homology arm starting at an *EcoR* V site ~1 kb 5′ of exon 2 and ending ~100 bp 5′ of exon 5; (2) *loxP* sites ~100 bp 5′ of exon 5 and 3′ of exon 6, with a *Frt-PGK-Neo-Frt* (*FNF*) cassette adjacent to the 5′ *loxP* site and (3) a ~3.5 kb 3′ homology arm starting ~100 bp 3′ of exon 6 and ending at an Apa I site in exon 8 (Fig. 1). The *loxP* sites are 640 bp apart. The targeting sequences were inserted into a vector with a *PGK* promoter and Herpes Simplex Virus Thymidine Kinase coding region for negative selection with ganciclovir. Following electroporation of R1 ES cells, positive selection with G418 and negative selection with ganciclovir correctly targeted ES clones were identified by southern blotting with probes distal to the 5′ and 3′ homology arms. Correctly targeted clones with a normal karyotype were injected into mouse blastocysts. To create the constitutive null allele (*Kif11*$^{-}$), the original *Kif11* targeted allele with *FNF* still present was subjected to germline Cre-mediated recombination by crossing to *Sox2-Cre*. To generate the *Kif11*^{CKO} allele, the *FNF* cassette was excised by crossing to germline *Flp*-expressing mice (*R26-Flp*). Genotyping to distinguish WT and *Kif11*^{CKO} alleles with a single PCR reaction was performed with a pair of primers flanking the 3′ loxP site [sense: ACTGCAGCAACCTTGATGAATGCTT (PMS1134) and antisense: CAATCTTCCAGTATTGCGAGCCTC (PMS1161)]. Three PCR primers were used in two separate PCR reactions to distinguish the WT *Kif11* allele, the *Kif11*^{CKO} allele and the *Kif11* null allele resulting from Cre-mediated recombination of the *Kif11*^{CKO} allele (Supplementary Material, Fig. S1): GATGGGAGGTGTAGCTGAGTAGTA (PMS1181), AGATTTCCAATAGGGACACTTTAACTG (JN4435) and ATGGTTGATTTTGAGACACAGTC (JN4437). PCR conditions were 1 × 94°C for 4 min, 35 × (94°C for 10 s; 63°C for 30 s; 72°C for 30 s) and 1 × 72°C for 7 min.

Antibodies and other reagents

The following antibodies were used for tissue immunohistochemistry and immunoblotting: rat anti-mouse PLVAP (MECA-32; BD Biosciences 553 849); mouse anti-Claudin5, Alexa Fluor 488 conjugate (Thermo Fisher Scientific 352 588); rabbit mAb anti-LEF1 (Cell Signaling Technologies C12A5); Texas Red

Streptavidin (Vector Laboratories SA-5006). Alexa Fluor-labeled secondary antibodies and GS Lectin (Isolectin GS-IB4) were from Thermo Fisher Scientific. Sulfo-NHS-biotin was from Thermo Fisher Scientific (21217).

Tissue processing and immunohistochemistry

Tissues were prepared and processed for immunohistochemical analysis as described by Wang *et al.* (49) and Zhou *et al.* (58). Mice were injected intraperitoneally with Sulfo-NHS-biotin (100 µl of 20 mg/ml Sulfo-NHS-biotin in PBS for P8–P12 mice and 200 µl of 20 mg/ml Sulfo-NHS-biotin in PBS for P31 mice) ∼30 min prior to sacrifice. Mice were deeply anesthetized with ketamine and xylazine and then perfused via the cardiac route with 1% PFA in PBS without calcium or magnesium, and the brains were dissected and dehydrated in 100% MeOH overnight at 4°C. Tissues were re-hydrated the following day in 1× PBS at 4°C for at least 3 h before embedding in 3% agarose. Tissue sections of 100–200 µm thickness were cut using a vibratome (Leica). For retina flatmounts, intact eyes were immersion fixed in 1% PFA in PBS at room temperature for 1 h, and then, the retinas were dissected and processed as described below.

Sections were incubated overnight with primary antibodies or Texas Red streptavidin diluted in 1× PBSTC (1× PBS + 1% Triton X-100 + 0.1 mM $CaCl_2$) + 10% normal goat serum (NGS). Incubation and washing steps were performed at 4°C. Sections were washed at least three times with 1× PBSTC over the course of 6 h and subsequently incubated overnight with secondary antibodies diluted in 1× PBSTC +10% NGS. If a primary rat antibody was used, secondary antibodies were additionally incubated with 1% normal mouse serum as a blocking agent. The next day, sections were washed at least three times with 1× PBSTC over the course of 6 h and flat mounted using Fluoromount G (EM Sciences 17 984-25). Sections were imaged using a Zeiss LSM700 confocal microscope and processed with ImageJ, Adobe Photoshop and Adobe Illustrator software.

4HT preparation and administration

Solid 4HT (Sigma-Aldrich H7904) was dissolved in an ethanol: sunflower seed oil (Sigma-Aldrich S5007) mixture (1:10 volume:volume) to a final concentration of 2 mg/ml and stored in aliquots at −80°C. All injections were performed intraperitoneally.

Quantification of retinal vascular growth and cerebellar EC vascular density

For quantifying the distance from the optic disc to the vascular front, four distance measurements at 90-degree intervals were made from each image of a flat-mounted retina. For quantifying the density of blood vessels at the granule cell layer/molecular layer junction, 100 µm thick sagittal vibratome sections were stained with GS-lectin and DAPI. Confocal images were scanned at 10 µm intervals along the Z-axis, and four of these scans were Z-stacked. Starting with each Z-stacked image (as seen in Fig. 5), the Adobe Illustrator pencil tool was used to first trace the length of the granule cell layer/molecular layer junction for each of the seven cerebellar folia and then to trace those regions of the granule cell layer/molecular layer junction that included a blood vessel. The length the traces for each folium was quantified by calculating its pixel coverage as a fraction of a standard rectangular area, using ImageJ. For the granule cell layer/molecular layer junction of each folium, the vascularized length was divided by the total length to yield the fraction of the granule cell layer/molecular layer junction that was vascularized. MATLAB and Excel were used to generate plots and to perform statistical analysis. The mean ± standard deviations are shown. Statistical significance was determined by the unpaired *t* test, using the mean values for each mouse.

Supplementary Material

Supplementary Material is available at *HMG* online.

Acknowledgements

The authors thank Chip Hawkins, Ann Lawler and Johnisha Witherspoon (Johns Hopkins Transgenic Core Facility) for ES cell injection, Dr Maketo Taketo (Kyoto University) for the *Ctnnb1*^{flex3} mice and Drs. Chris Cho, Amir Rattner and Jie Wang for assistance and helpful discussions.

Funding

This work was supported by the Howard Hughes Medical Institute.

Conflict of Interest: None declared.

References

1. Gilmour, D.F. (2015) Familial exudative vitreoretinopathy and related retinopathies. *Eye (Lond.)*, **29**, 1–14.
2. Sun, Y. and Smith, L.E.H. (2018) Retinal vasculature in development and diseases. *Annu. Rev. Vis. Sci.*, **4**, 101–122.
3. Nikopoulos, K., Venselaar, H., Collin, R.W., Riveiro-Alvarez, R., Boonstra, F.N., Hooymans, J.M., Mukhopadhyay, A., Shears, D., van Bers, M., de Wijs, I.J. *et al.* (2010) Overview of the mutation spectrum in familial exudative vitreoretinopathy and Norrie disease with identification of 21 novel variants in FZD4, LRP5, and NDP. *Hum. Mutat.*, **31**, 656–666.
4. Rao, F.Q., Cai, X.B., Cheng, F.F., Cheng, W., Fang, X.L., Li, N., Huang, X.F., Li, L.H. and Jin, Z.B. (2017) Mutations in LRP5,FZD4, TSPAN12, NDP, ZNF408, or KIF11 genes account for 38.7% of Chinese patients with familial exudative vitreoretinopathy. *Invest. Ophthalmol. Vis. Sci.*, **58**, 2623–2629.
5. Tang, M., Sun, L., Hu, A., Yuan, M., Yang, Y., Peng, X. and Ding, X. (2017) Mutation spectrum of the LRP5, NDP, and TSPAN12 genes in Chinese patients with familial exudative vitreoretinopathy. *Invest. Ophthalmol. Vis. Sci.*, **58**, 5949–5957.
6. Li, J.K., Li, Y., Zhang, X., Chen, C.L., Rao, Y.Q., Fei, P., Zhang, Q., Zhao, P. and Li, J. (2018) Spectrum of variants in 389 Chinese probands with familial exudative vitreoretinopathy. *Invest. Ophthalmol. Vis. Sci.*, **59**, 5368–5381.
7. Ye, X., Wang, Y. and Nathans, J. (2010) The Norrin/Frizzled4 signaling pathway in retinal vascular development and disease. *Trends Mol. Med.*, **16**, 417–425.
8. Stenman, J.M., Rajagopal, J., Carroll, T.J., Ishibashi, M., McMahon, J. and McMahon, A.P. (2008) Canonical Wnt signaling regulates organ-specific assembly and differentiation of CNS vasculature. *Science*, **322**, 1247–1250.
9. Daneman, R., Agalliu, D., Zhou, L., Kuhnert, F., Kuo, C.J. and Barres, B.A. (2009) Wnt/beta-catenin signaling is required for CNS, but not non-CNS, angiogenesis. *Proc. Natl. Acad. Sci. U. S. A.*, **106**, 6422–6422.
10. Zhou, Y. and Nathans, J. (2014) Gpr124 controls CNS angiogenesis and blood-brain barrier integrity by promoting

ligand-specific canonical Wnt signaling. *Dev. Cell*, **31**, 248–256.
11. Posokhova, E., Shukla, A., Seaman, S., Volate, S., Hilton, M.B., Wu, B., Morris, H., Swing, D.A., Zhou, M., Zudaire, E. *et al.* (2015) GPR124 functions as a WNT7-specific coactivator of canonical β-catenin signaling. *Cell Rep.*, **10**, 123–130.
12. Vanhollebeke, B., Stone, O.A., Bostaille, N., Cho, C., Zhou, Y., Maquet, E., Gauquier, A., Cabochette, P., Fukuhara, S., Mochizuki, N. *et al.* (2015) Tip cell-specific requirement for an atypical Gpr124- and Reck-dependent Wnt/β-catenin pathway during brain angiogenesis. *elife*, **4**, e06489.
13. Cho, C., Smallwood, P.M. and Nathans, J. (2017) Reck and Gpr124 are essential receptor cofactors for Wnt7a/Wnt7b-specific Signaling in mammalian CNS angiogenesis and blood-brain barrier regulation. *Neuron*, **95**, 1056–1073.
14. Eubelen, M., Bostaille, N., Cabochette, P., Gauquier, A., Tebabi, P., Dumitru, A.C., Koehler, M., Gut, P., Alsteens, D., Stainier, D.Y.R., Garcia-Pino, A. and Vanhollebeke, B. (2018) A molecular mechanism for Wnt ligand-specific signaling. *Science*, **361**, 6403.
15. Wang, Y., Cho, C., Williams, J., Smallwood, P.M., Zhang, C., Junge, H.J. and Nathans, J. (2018) Interplay of the Norrin and Wnt7a/Wnt7b signaling systems in blood-brain barrier and blood-retina barrier development and maintenance. *Proc. Natl. Acad. Sci. U. S. A.*, **115**, E11827–E11836.
16. Smith, S.E., Mullen, T.E., Graham, D., Sims, K.B. and Rehm, H.L. (2012) Norrie disease: extraocular clinical manifestations in 56 patients. *Am. J. Med. Genet. A*, **158A**, 1909–1917.
17. Maupin, K.A., Droscha, C.J. and Williams, B.O. (2013) A comprehensive overview of skeletal phenotypes associated with alterations in Wnt/β-catenin Signaling in humans and mice. *Bone Res.*, **1**, 27–71.
18. Panagiotou, E.S., Sanjurjo Soriano, C., Poulter, J.A., Lord, E.C., Dzulova, D., Kondo, H., Hiyoshi, A., Chung, B.H., Chu, Y.W., Lai, C.H.Y. *et al.* (2017) Defects in the cell signaling mediator β-catenin cause the retinal vascular condition FEVR. *Am. J. Hum. Genet.*, **100**, 960–968.
19. Sun, W., Xiao, X., Li, S., Jia, X., Wang, P. and Zhang, Q. (2019) Germline mutations in CTNNB1 associated with syndromic FEVR or Norrie disease. *Invest. Ophthalmol. Vis. Sci.*, **60**, 93–97.
20. Tucci, V., Kleefstra, T., Hardy, A., Heise, I., Maggi, S., Willemsen, M.H., Hilton, H., Esapa, C., Simon, M., Buenavista, M.T. *et al.* (2014) Dominant β-catenin mutations cause intellectual disability with recognizable syndromic features. *J. Clin. Invest.*, **124**, 1468–1482.
21. Kuechler, A., Willemsen, M.H., Albrecht, B., Bacino, C.A., Bartholomew, D.W., van Bokhoven, H., van den Boogaard, M.J., Bramswig, N., Büttner, C., Cremer, K. *et al.* (2015) De novo mutations in beta-catenin (CTNNB1) appear to be a frequent cause of intellectual disability: expanding the mutational and clinical spectrum. *Hum. Genet.*, **134**, 97–109.
22. Kharbanda, M., Pilz, D.T., Tomkins, S., Chandler, K., Saggar, A., Fryer, A., McKay, V., Louro, P., Smith, J.C., Burn, J. *et al.* (2017) Clinical features associated with CTNNB1 de novo loss of function mutations in ten individuals. *Eur. J. Med. Genet.*, **60**, 130–135.
23. Valenta, T., Hausmann, G. and Basler, K. (2012) The many faces and functions of β-catenin. *EMBO J.*, **31**, 2714–2736.
24. Limwongse, C., Wyszynski, R.E., Dickerman, L.H. and Robin, N.H. (1999) Microcephaly-lymphedema-chorioretinal dysplasia: a unique genetic syndrome with variable expression and possible characteristic facial appearance. *Am. J. Med. Genet.*, **86**, 215–218.
25. Hazan, F., Ostergaard, P., Ozturk, T., Kantekin, E., Atlihan, F., Jeffery, S. and Ozkinay, F. (2012) A novel KIF11 mutation in a Turkish patient with microcephaly, lymphedema, and chorioretinal dysplasia from a consanguineous family. *Am. J. Med. Genet. A*, **158A**, 1686–1689.
26. Kelly, M.N., Khuddus, N., Motamarry, S. and Tuli, S. (2012) Microcephaly, lymphedema, chorioretinal dysplasia (MLCRD) syndrome. *J. Pediatr. Health Care*, **26**, 306–311.
27. Ostergaard, P., Simpson, M.A., Mendola, A., Vasudevan, P., Connell, F.C., van Impel, A., Moore, A.T., Loeys, B.L., Ghalamkarpour, A., Onoufriadis, A. *et al.* (2012) Mutations in KIF11 cause autosomal-dominant microcephaly variably associated with congenital lymphedema and chorioretinopathy. *Am. J. Hum. Genet.*, **90**, 356–362.
28. Mirzaa, G.M., Enyedi, L., Parsons, G., Collins, S., Medne, L., Adams, C., Ward, T., Davitt, B., Bicknese, A., Zackai, E. *et al.* (2014) Congenital microcephaly and chorioretinopathy due to de novo heterozygous KIF11 mutations: five novel mutations and review of the literature. *Am. J. Med. Genet. A*, **164A**, 2879–2886.
29. Mears, K., Bakall, B., Harney, L.A., Penticoff, J.A. and Stone, E.M. (2015) Autosomal dominant microcephaly associated with congenital lymphedema and chorioretinopathy due to a novel mutation in KIF11. *JAMA Ophthalmol.*, **133**, 720–721.
30. Balikova, I., Robson, A.G., Holder, G.E., Ostergaard, P., Mansour, S. and Moore, A.T. (2016) Ocular manifestations of microcephaly with or without chorioretinopathy, lymphedema or intellectual disability (MCLID) syndrome associated with mutations in KIF11. *Acta Ophthalmol.*, **94**, 92–98.
31. Birtel, J., Gliem, M., Mangold, E., Tebbe, L., Spier, I., Müller, P.L., Holz, F.G., Neuhaus, C., Wolfrum, U., Bolz, H. and Charbel Issa, P. (2017) Novel insights into the phenotypical spectrum of KIF11-associated retinopathy, including a new form of retinal ciliopathy. *Invest. Ophthalmol. Vis. Sci.*, **58**, 3950–3959.
32. Robitaille, J.M., Gillett, R.M., LeBlanc, M.A., Gaston, D., Nightingale, M., Mackley, M.P., Parkash, S., Hathaway, J., Thomas, A., Ells, A. *et al.* (2014) Phenotypic overlap between familial exudative vitreoretinopathy and microcephaly, lymphedema, and chorioretinal dysplasia caused by KIF11 mutations. *JAMA Ophthalmol.*, **132**, 1393–1399.
33. Hu, H., Xiao, X., Li, S., Jia, X., Guo, X. and Zhang, Q. (2016) KIF11 mutations are a common cause of autosomal dominant familial exudative vitreoretinopathy. *Br. J. Ophthalmol.*, **100**, 278–283.
34. Li, J.K., Fei, P., Li, Y., Huang, Q.J., Zhang, Q., Zhang, X., Rao, Y.Q., Li, J. and Zhao, P. (2016) Identification of novel KIF11 mutations in patients with familial exudative vitreoretinopathy and a phenotypic analysis. *Sci. Rep.*, **6**, 26564.
35. Karjosukarso, D.W., Cremers, F.P.M., van Nouhuys, C.E. and Collin, R.W.J. (2018) Detection and quantification of a KIF11 mosaicism in a subject presenting familial exudative vitreoretinopathy with microcephaly. *Eur. J. Hum. Genet.*, **26**, 1819–1823.
36. Blangy, A., Lane, H.A., d'Herin, P., Harper, M., Kress, M. and Nigg, E.A. (1995) Phosphorylation by p34(cdc2) regulates spindle association of human Eg5, a kinesin-related motor essential for bipolar spindle formation in vivo. *Cell*, **83**, 1159–1169.
37. Ferenz, N.P., Gable, A. and Wadsworth, P. (2010) Mitotic functions of kinesin-5. *Semin. Cell Dev. Biol.*, **21**, 255–259.
38. Bartoli, K.M., Jakovljevic, J., Woolford, J.L., Jr. and Saunders, W.S. (2011) Kinesin molecular motor Eg5 functions during polypeptide synthesis. *Mol. Biol. Cell*, **22**, 3420–3430.

39. Wakana, Y., Villeneuve, J., van Galen, J., Cruz-Garcia, D., Tagaya, M. and Malhotra, V. (2013) Kinesin-5/Eg5 is important for transport of CARTS from the trans-Golgi network to the cell surface. *J. Cell Biol.*, **202**, 241–250.
40. Falnikar, A., Tole, S. and Baas, P.W. (2011) Kinesin-5, a mitotic microtubule-associated motor protein, modulates neuronal migration. *Mol. Biol. Cell*, **22**, 1561–1574.
41. Kahn, O.I., Sharma, V., González-Billault, C. and Baas, P.W. (2015) Effects of kinesin-5 inhibition on dendritic architecture and microtubule organization. *Mol. Biol. Cell*, **26**, 66–77.
42. Freixo, F., Martinez Delgado, P., Manso, Y., Sánchez-Huertas, C., Lacasa, C., Soriano, E., Roig, J. and Lüders, J. (2018) NEK7 regulates dendrite morphogenesis in neurons via Eg5-dependent microtubule stabilization. *Nat. Commun.*, **9**, 2330.
43. Rath, O. and Kozielski, F. (2012) Kinesins and cancer. *Nat. Rev. Cancer*, **12**, 527–539.
44. Myers, S.M. and Collins, I. (2016) Recent findings and future directions for interpolar mitotic kinesin inhibitors in cancer therapy. *Future Med. Chem.*, **8**, 463–489.
45. Castillo, A. and Justice, M.J. (2007) The kinesin related motor protein, Eg5, is essential for maintenance of pre-implantation embryogenesis. *Biochem. Biophys. Res. Commun.*, **357**, 694–699.
46. Chauvière, M., Kress, C. and Kress, M. (2008) Disruption of the mitotic kinesin Eg5 gene (Knsl1) results in early embryonic lethality. *Biochem. Biophys. Res. Commun.*, **372**, 513–519.
47. Luhmann, U.F., Lin, J., Acar, N., Lammel, S., Feil, S., Grimm, C., Seeliger, M.W., Hammes, H.P. and Berger, W. (2005) Role of the Norrie disease pseudoglioma gene in sprouting angiogenesis during development of the retinal vasculature. *Invest. Ophthalmol. Vis. Sci.*, **46**, 3372–3382.
48. Ye, X., Wang, Y., Cahill, H., Yu, M., Badea, T.C., Smallwood, P.M., Peachey, N.S. and Nathans, J. (2009) Norrin, frizzled-4, and Lrp5 signaling in endothelial cells controls a genetic program for retinal vascularization. *Cell*, **139**, 285–298.
49. Wang, Y., Rattner, A., Zhou, Y., Williams, J., Smallwood, P.M. and Nathans, J. (2012) Norrin/Frizzled4 signaling in retinal vascular development and blood brain barrier plasticity. *Cell*, **151**, 1332–1344.
50. Rattner, A., Yu, H., Williams, J., Smallwood, P.M. and Nathans, J. (2013) Endothelin-2 signaling in the neural retina promotes the endothelial tip cell state and inhibits angiogenesis. *Proc. Natl. Acad. Sci. U. S. A.*, **110**, E3830–E3839.
51. Rattner, A., Wang, Y., Zhou, Y., Williams, J. and Nathans, J. (2014) The role of the hypoxia response in shaping retinal vascular development in the absence of Norrin/Frizzled4 signaling. *Invest. Ophthalmol. Vis. Sci.*, **55**, 8614–8625.
52. Heng, J.S., Rattner, A., Stein-O'Brien, G.L., Winer, B.L., Jones, B.W., Vernon, H.J., Goff, L.A. and Nathans, J. (2019) Hypoxia tolerance in the Norrin-deficient retina and the chronically hypoxic brain studied at single-cell resolution. *Proc. Natl. Acad. Sci. U. S. A.*, **116**, 9103–9114.
53. Chow, B.W. and Gu, C. (2017) Gradual suppression of transcytosis governs functional blood-retinal barrier formation. *Neuron*, **93**, 1325–1333.
54. Stan, R.V., Tkachenko, E. and Niesman, I.R. (2004) PV1 is a key structural component for the formation of the stomatal and fenestral diaphragms. *Mol. Biol. Cell*, **15**, 3615–3630.
55. Kaur, C., Foulds, W.S. and Ling, E.A. (2008) Blood-retinal barrier in hypoxic ischaemic conditions: basic concepts, clinical features and management. *Prog. Retin. Eye Res.*, **27**, 622–647.
56. Sabbagh, M.F., Heng, J.S., Luo, C., Castanon, R.G., Nery, J.R., Rattner, A., Goff, L.A., Ecker, J.R. and Nathans, J. (2018) Transcriptional and epigenomic landscapes of CNS and non-CNS vascular endothelial cells. *elife*, **7**, e36187.
57. Wang, Y., Sabbagh, M.F., Gu, X., Rattner, A., Williams, J. and Nathans, J. (2019) Beta-catenin signaling regulates barrier-specific gene expression in circumventricular organ and ocular vasculatures. *elife*, **8**, e43257.
58. Zhou, Y., Wang, Y., Tischfield, M., Williams, J., Smallwood, P.M., Rattner, A., Taketo, M.M. and Nathans, J. (2014) Canonical WNT signaling components in vascular development and barrier formation. *J. Clin. Invest.*, **124**, 3825–3846.
59. Chizhikov, V. and Millen, K.J. (2003) Development and malformations of the cerebellum in mice. *Mol. Genet. Metab.*, **80**, 54–65.
60. van Heesbeen, R.G., Tanenbaum, M.E. and Medema, R.H. (2014) Balanced activity of three mitotic motors is required for bipolar spindle assembly and chromosome segregation. *Cell Rep.*, **8**, 948–956.
61. Gayek, A.S. and Ohi, R. (2014) Kinetochore-microtubule stability governs the metaphase requirement for Eg5. *Mol. Biol. Cell*, **25**, 2051–2060.
62. Tanenbaum, M.E., Macůrek, L., Janssen, A., Geers, E.F., Alvarez-Fernández, M. and Medema, R.H. (2009) Kif15 cooperates with eg5 to promote bipolar spindle assembly. *Curr. Biol.*, **19**, 1703–1711.
63. Sturgill, E.G., Norris, S.R., Guo, Y. and Ohi, R. (2016) Kinesin-5 inhibitor resistance is driven by kinesin-12. *J. Cell Biol.*, **213**, 213–227.
64. Exertier, P., Javerzat, S., Wang, B., Franco, M., Herbert, J., Platonova, N., Winandy, M., Pujol, N., Nivelles, O., Ormenese, S. *et al.* (2013) Impaired angiogenesis and tumor development by inhibition of the mitotic kinesin Eg5. *Oncotarget*, **4**, 2302–2316.
65. Claxton, S., Kostourou, V., Jadeja, S., Chambon, P., Hodivala-Dilke, K. and Fruttiger, M. (2008) Efficient, inducible Cre-recombinase activation in vascular endothelium. *Genesis*, **46**, 74–80.
66. Hayashi, S., Lewis, P., Pevny, L. and McMahon, A.P. (2002) Efficient gene modulation in mouse epiblast using a Sox2Cre transgenic mouse strain. *Gene Expr. Patterns*, **2**, 93–97.
67. Farley, F.W., Soriano, P., Steffen, L.S. and Dymecki, S.M. (2000) Widespread recombinase expression using FLPeR (flipper) mice. *Genesis*, **28**, 106–110.
68. Harada, N., Tamai, Y., Ishikawa, T., Sauer, B., Takaku, K., Oshima, M. and Taketo, M.M. (1999) Intestinal polyposis in mice with a dominant stable mutation of the beta-catenin gene. *EMBO J.*, **18**, 5931–5942.